Chalcogenide Letters Vol. 17, No. 3, March 2020, p. 123 - 132

COMPARATIVE STUDY OF THE MULTI-JUNCTION CIGS BASED SOLAR CELL PERFORMANCE WITH DIFFERENT MODES

T. BELHADJI[a*], B. DENNAI[b,*]
[a]*Laboratory of Semiconductor Devices Physics, University Tahri Mohammed of Bechar, Algeria*
[b]*Laboratory Smart grid & Renewable Energy, Faculty of Exact Sciences, University Tahri Mohammed, Bechar, Algeria*

Today, The CIGS industrial sector emerges in the photovoltaic domain. Many significant enhancements are possible allowing to better ameliorate the solar cell performances. Thin-layer cells are second generation cells which are the result of the first generation cells evolution made of Silicium but with layer of extreme thickness [1].A simulation will be carried out for multi-color associations of photo batteries coupled in dichroic, tandem or cascade mode based on (CuGaSe2), (CuIn1-xGaxSe2) and their variants.A study of physical parameters influence and different layers will be done in order to determine the system of converting a larger part of solar spectrum leading to a high efficiency.

(Received December 21, 2019; Accepted March 11, 2020)

Keywords: CIGS, Simulation, Tandem, Dichroic, Cascade, Solar cell, Efficiency

1. Introduction

The Thin- film solar cells are diodes of large area tailored to enable and maximize the absorption of light within a short distance from the space charge region of solar cells and provide a numerous productivity advantages in comparison with the bulk silicon devices which are complicated and highly costing to produce [2]

The CIGS as a thin layer is a versatile and efficient material according to the world records. As Si and CdTe thin-film cells have efficiently improved, CIGS thin-film cells have, in parallel, evolved and remained the leading technologies with distinct advantages. Polycrystalline CIGS technologies achieved higher efficiency than polycrystalline silicon and cost low [3].

Solar cells of Multi-junctions (MJ) are promising technologies that attained a high efficiency conversion of sunlight to electricity but they can be affected by the underlying mechanisms causing resistive losses [4].

In this work, a comparison was carried out between the following three modes (dichroic, tandem and cascade) on multi-junction CIGS based dispositive.

2. Cell structure and material properties

2.1. Cell structure

A solar cell with multi-junction is simply defined as a cell containing two or more single-junction semiconductors. The layer of semiconductor is of different band-gaps energy. The band-gap energy is high on the upper surface whereas on the bottom surface, the band-gap energy is low. In our studies, we have three structures; each structure expresses a mode of multi-junction solar cells (Fig.1, 2, 3).

In Fig. 1 the proposed solar cell structure of tandem mode comprises two junctions. Top cell (CGS) with $Eg_{(CGS)} = 1.67eV$, and a bottom cell (CIGS) with $Eg_{(CIGS)} = 1.21eV$. These two cells are optically and electrically connected with a transparent conducting oxide layer of ZnO [5].

* Corresponding authors: deennai_benmoussa@yahoo.com

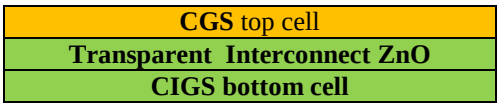

Fig. 1. Tandem solar cell with CGS/CIGS sub-cells connected by transparent interconnect ZnO.

In Fig. 2 the suggested solar cell structure of cascade mode, the n+/p+ tunnel junction is sandwiched between two cells. One top sub-cell (CGS) with $\mathrm{Eg}_{(\mathrm{CGS})} = 1.67\mathrm{eV}$ and bottom sub-cell (CIGS) with $\mathrm{Eg}_{(\mathrm{CIGS})} = 1.21\mathrm{eV}$.

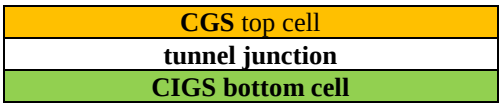

Fig. 2. Tandem solar cell with CGS/CIGS sub-cells connected by tunnel junction.

In Fig.3 one of the configurations said 'dichroic ', the solar spectrum incident is fractionated by optical system separator of dichotic mirrors of several portions corresponding to spectrum sub-bands. Each of the portions is re-directed towards the solar cell of different types (CGS) and (CIGS) in an optimized way to a given photon energy taking into account that $\mathrm{Eg}_{(\mathrm{CGS})} = 1.67\mathrm{eV}, \mathrm{Eg}_{(\mathrm{CIGS})} = 1.21\mathrm{eV}$

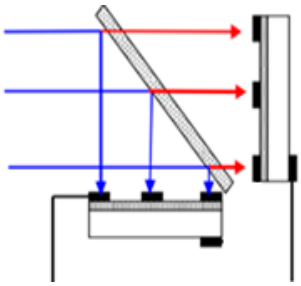

Fig.3. Schematic of electrical coupling of two cells in series.

2.2. Parameters for simulation

The Table 1 below shows the material properties of each of the three layers that are necessary for modeling. The layers are respectively; n+ ZnO (window), n- Cds and P- CIGS. The transmission and reflection of the back and the front contacts should be set before simulation is done. It also displays the parameters and the base parameters of the simulation that are used in the study. [6]

Table 1. The parameters for the cigs-based solar cell at 300k.

Film **Parameters**	**ZnO**	**Cds**	**CGS**	**CIGS**
Thickness(nm)	200	50	3000	3000
Relative permittivity ,ε	9	10	13.6	13.6
Electron mobilityμ_n (cm²/Vs)	100	100	100	100
Hole mobility μ_p(cm²/Vs)	31	25	25	25
Density of carriers, n or p (cm^{-3})	1*e16	1*e17	2*e16	2*e16
Layer band gap,E_g(eV)	3.3	2.42	1.67	1.21
Conduction band effective density of states,N_c (cm^{-3})	3.1*e18	2.2*e18	2.2*e18	2.2*e18
Valence band effective density of states,$N_v(cm^{-3})$	1.8*e19	1.8*e19	1.8*e19	1.8*e19
Electron affinity, χ (eV)	4.55	4.4	4.5	4.5

3. Numerical simulation

In this part, calculations were all performed under the sun illumination (AM=1.5) and a temperature of (300 K) conditions using the one-diode ideal model. For convenience, several simplifying assumptions were made including no-series resistance, reflection losses and contact shadowing.

The density totality of photo current of each cell with its illumination is given by:[7]

$$j_{ph} = j_n + j_P + j_{ZEC} \tag{1}$$

Where: j_n is the density of photo current in the base region that is expressed by:

$$j_n = \left(q\frac{F(1-R)\alpha_2 L_n}{\alpha_2^2 L_n^2 - 1}\right)\exp(-\alpha_1(x_n + w_1) - \alpha_2 w_2) \times \left[\alpha_2 L_n - \frac{\frac{s_n L_n}{D_n} + \left(ch\left(\frac{H\prime}{L_n}\right) - \exp(-\alpha_2 H')\right) + sh\left(\frac{H\prime}{L_n}\right) + \alpha_2 L_n \exp(-\alpha_2 H')}{\frac{s_n L_n}{D_n} sh\left(\frac{H\prime}{L_n}\right) + ch\left(\frac{H\prime}{L_n}\right)}\right] \tag{2}$$

j_p: The photo current density in the emitter region that is expressed by:

$$j_p = \left(q\frac{F(1-R)\alpha_1 L_P}{\alpha_1^2 L_P^2 - 1}\right)\left[\frac{\frac{s_p L_p}{D_p} + \alpha_1 L_P - exp(-\alpha_1 x_n)\left(\frac{s_p L_p}{D_p} ch\left(\frac{x_n}{L_P}\right) + sh\left(\frac{x_n}{L_P}\right)\right)}{\frac{s_p L_p}{D_p} sh\left(\frac{x_n}{L_P}\right) + ch\left(\frac{x_n}{L_P}\right)} - \alpha_1 L_P\, exp(-\alpha_1 x_n)\right] \tag{3}$$

j_{ZEC}: The photo current density in the space zone that is expressed by:

$$j_{ZEC} = qF(1-R)e^{-\alpha_1 x_j}((1 - e^{-\alpha_1 w_1}) + e^{-\alpha_1 w_1}(1 - e^{-\alpha_2 w_2})) \tag{4}$$

Open circuit tension is given by:

$$V_{OC} = \frac{KT}{q} \times \; Log\; \left(1 + \frac{I_{ph}}{I_0}\right) \tag{5}$$

4. PV characteristics

4.1. Electrical characteristics of the single solar cell

The tension supplied to circuit by a solar cell under illumination of charge resistance is maximal for an operational point $P_m(I_m, V_m)$ of current voltage curve. At this point, it is approximately written [8]:

$$V_{mp} = V_{OC} - \frac{K.T}{q} \times Log\left(1 + \frac{q.V_{mp}}{K.T}\right) \quad (6)$$

$$I_{mp} = \left[I_{ph} + j_0\left(e^{\frac{q.V_{mp}}{K.T}} - 1\right)\right] \quad (7)$$

The maximum energetic efficiency is expressed by:

$$\eta_m = \frac{P_{max}}{P_{in}} = \frac{I_m.V_m}{P_{in}} \quad (8)$$

P_{in}: Theincidental power of solar rays to the ground.

4.2. Electrical characteristics of the tandem mode (stacked)

In this mode, the cells are electrically linked to each other. It must be noted that the same current goes through all of the cells and that the total electrical tension at the terminals V_{tan} of the device will simply be the sum of the tensions at the terminals of each cell.

$V_{tan} = V_1 + V_2$ With V_1, V_2 The voltage for top cell and bottom cell respectively.

After determining the operating point $I_{mk}; V_{mk}$ (K=1,2) of the independent cells, an applied series current I equals to the smallest of the currentsI_{mk} that is to say $I = \inf(I_{mk})$.

Hence, the global efficiency can be calculated as follows:

$$\eta = \frac{V_{tan}.I}{P_{in}} = \frac{(V_1+V_2).\ \inf(I_{mk})}{P_{in}} \quad (9)$$

4.3. Electrical characteristics of the mode dichroic solar cell

For the dichroic mode, there are two efficiency calculations:

If the cells are independent it is called the independent system. Therefore, the output of the solar cells in the dichroic mode equals to:

$$\eta_{mk} = \frac{P_{max\,k}}{P_{in}} = \frac{I_{mk}.V_{mk}}{P_{in}} \quad (10)$$

When the cells are connected to each other by a conductive wire, it is said electric coupling. It is the same case we have in tandem mode.

4.4. Electrical characteristics of the monolithic cascade solar cell

As mentioned above, this multi-junction solar cell is composed of two solar cells that are electrified in series with a tunnel junction. Thus, the tension at the terminal of cascade is deduced by:

$V_{cas} = V_1 + V_2 - V_{th}$ $with$ V_1, V_2The voltage of tunnel junction and the flowing current in the multi- junction cell is the weakest current among all junction currents:

$$I = \inf(I_{mk}) \quad (11)$$

The global efficiency will be:

$$\eta = \frac{V_{cas}.I}{P_{in}} = \frac{(V_1+V_2-V_{th}).\ \inf(I_{mk})}{P_{in}} \quad (12)$$

5. Results and discussion

In this work the simulation process is carried out in four steps. In the first one, we simulate every solar cell (top and bottom) separately. In the three remaining steps, we simulate the two cells optically related (stacked) for the three modes, tandem, cascade and dichroic respectively.

5.1. Simulation of the first cell CGS only

In this study, we use the solar cell composed of the following hetero-junction ZnO/CdS /CGS. The simplified diagram of the hetero structure is represented in Fig. 4.

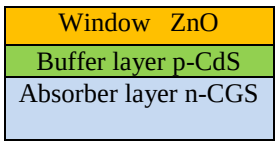

Fig. 4. Structure of a thin-film solar cell CGS.

Figs. 5, 6 and 7respectively represent the features: current- tension, power- tension and the spectral response in terms of the length of the CGS first solar cell.

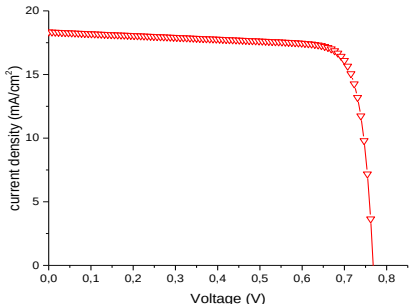

Fig.5. Current - tension Characteristic of CGS solar cell.

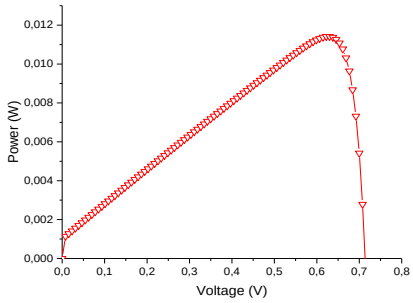

Fig. 6. Power-tension characteristic of the first CGS solar cell.

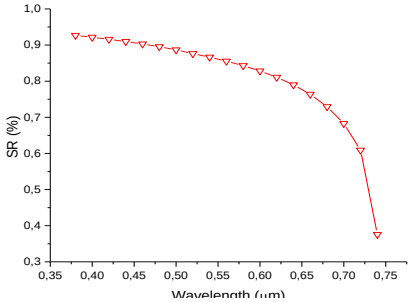

Fig. 7. Variation of spectral response in terms of wave length.

From the shape of Fig. 7, we notice that the first CGS solar cell absorbs a portion of spectrum with a wave length range between 0.36µm to 0.74 µm.

The photovoltaic parameters obtained from our simulation for the CGS solar cell are presented in the following Table2.

Table2.Photovoltaic parameters of CGS solar cell.

	j_{ph}(mA/cm²)	$V_{OC}(V)$	FF(%)	EFFICIENCY(%)
CGS single top cell	18.34	0.77	84	11.44

5.2. Simulation of the second CIGS cell only

In this simulation, the CIGS solar cell presented in Fig.8 with a rate of indium equaling 25%is analyzed.

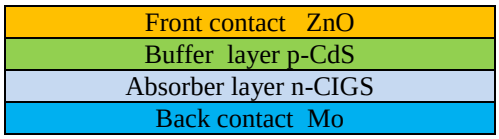

Fig. 8.*Structure of a thin-film solar cell CIGS.*

In Figs. 9,10 and11 are represented; the characteristic; current-tension (I-V), power-tension (P-V) and the spectral response in terms of wave length simulated of the second hetero junction CIGS device.

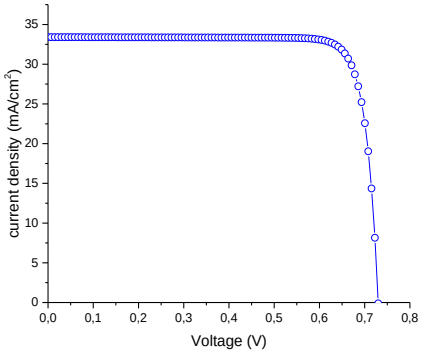

Fig. 9. Current - tension Characteristic of CIGS solar cell.

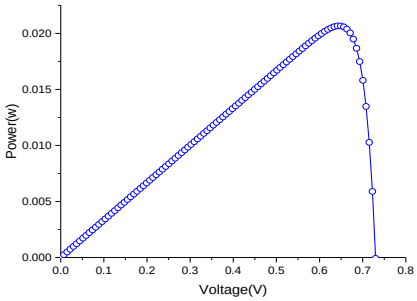

Fig.10. Power-tension characteristic of the second CIGS solar cell.

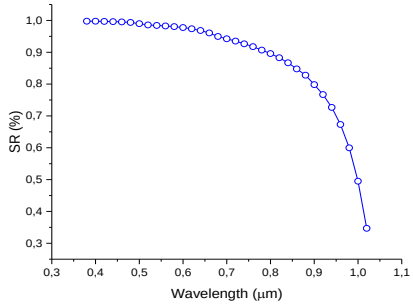

Fig. 11. Variation of spectral response in terms of wave length.

From the curve shape of Fig. 11, it is noticed that the first CIGS solar cell absorbs a part of the spectrum with a wave length range between 0.36 µm. to 1.02 µm.

The photovoltaic thicknesses of the second single cell are given in Table 3.

Table 3. Photovoltaic parameters of CIGS solar cell.

	$j_{ph}(\mathrm{mA/cm^2})$	$\mathrm{V_{OC}(V)}$	FF(%)	EFFICIENCY(%)
CIGS single bottom cell	33.41	0.73	77	20.66

5.3. Simulation of CGS/ CIGS multi-junction solar cell with tandem mode

The base structure of CGS/ CIGS double-junction solar cell is represented in Fig. 12. This conception consists of two solar cells: a top CGS solar cell of prohibitive large band($\mathrm{Eg_{(CGS)}} = 1.67\mathrm{eV}$) andbottom CIGS solar cell of prohibitive weak band ($\mathrm{Eg_{(CIGS)}} = 1.21\mathrm{eV}$) whose purpose is to absorb a large range of spectrum.

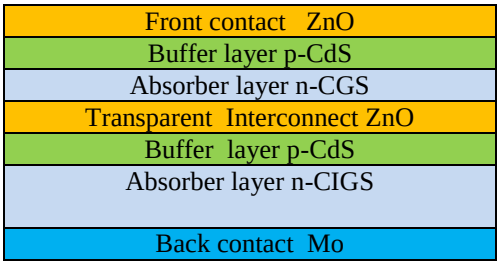

Fig. 12.Tandem solar cell with CGS/CIGS sub-cells connected by transparent interconnect ZnO.

The Fig. 13 and Fig. 14, shows the characteristics (V) and P (V) respectively, for the two independent cells and the CGS/CIGS solar cell with tandem.

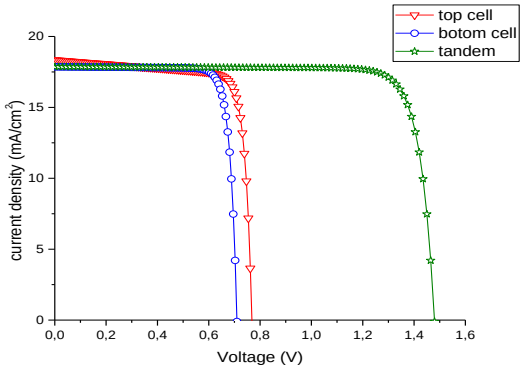

Fig. 13.Characteristics I (V) of the two tandem cells.

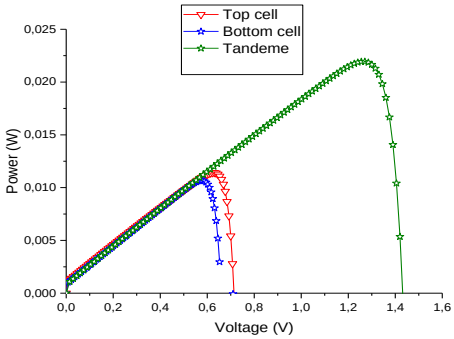

Fig. 14.CharacteristicsP (V) of the two tandem cells.

It is remarkably noticed that the system can develop a high tension that, in principle, is equal to the sum of all tensions of each component. The running current through the device is applied by the cell supplying the weakest current produced by the inferior CIGS cell in the couple.

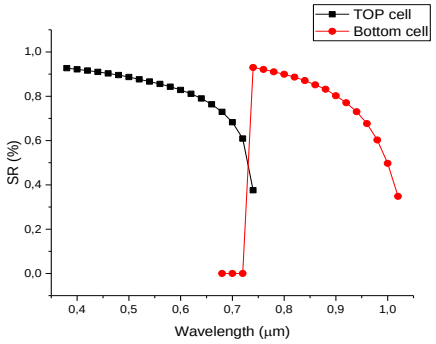

Fig. 15. Spectral response variation of the two cells in terms of the wave length.

From Fig. 15, it is clearly noticed that the largest part of the spectrum is absorbed by the first cell. However, the second cell (inferior cell) absorbs the rest of the spectrum which has not been absorbed by the first one.

Table4. Photovoltaic parameters of CGS/CIGS solar cell tandem.

	$j_{ph}(\mathrm{mA/cm^2})$	$V_{OC}(V)$	FF(%)	EFFICIENCY(%)
Tandem solar cell	17.86	1.48	84	22.35

5.4. Simulation of the CGS/ CIGS multi-junction solar cell with cascade mode.

In order to correspond the current between the sub-cells, the tunnel junctions are used to connect the sub-cells. For this reason, a two solar cell device is proposed with CGS (1,67eV) as a superior cell and CIGS (1.21 eV) as an inferior cell. The two cells are connected by a tunnel junction.

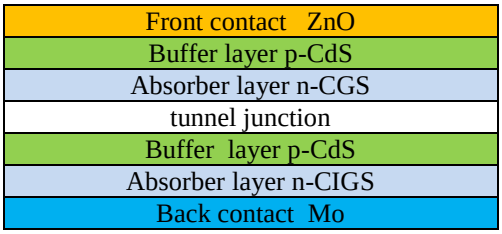

Fig. 16. Cascade solar cell with CGS/CIGS sub-cells connected by transparent interconnect tunnel junction.

The Figs. 17 and 18 respectively give the curves of the characteristics I(V) and P(V) of monolithic CGS/ CIGS multi-junction cell illustrating a very important increase of the performances in comparison with mono-spectral conversion.

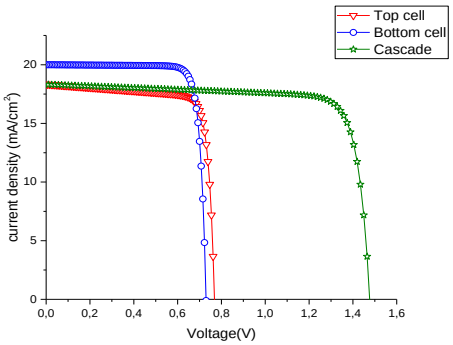

Fig.17Characteristics I(V) of the two cascade cells.

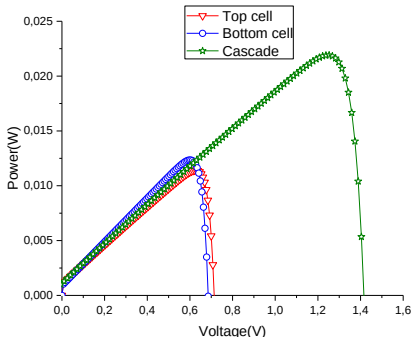

Fig. 18. Characteristics P(V) of the two cascade cells.

The running current in the device is supplied by a cell generating the weakest current. This latter is the current of the superior cell (CGS) in the couple cells contrary to what happened in the preceding cell.

The parameters of the CGS / CIGS cell of cascade mode drawn from the characteristics (J-V) are summarized in Table 5.

Table 5.Photovoltaic parameters of CGS/CIGS solar cell cascade.

	$j_{ph}(\mathrm{mA/cm^2})$	$V_{OC}(V)$	FF(%)	EFFICIENCY(%)
Cascade solar cell	18.34	1.46	77	23.75

5.5. Simulation of the CGS/ CIGS multi-junction solar cell with dichroic mode

In this system, the two optically stacked cells are electrically independent as indicated in Fig. 3.

The total efficiency is the sum of the efficiencies of both the first and the second cell.

$$\eta_{ind} = \eta_1 + \eta_2$$

From Table 2 and Table 3 the efficiency of independent system is:

$\eta_{ind} = 11.44 + 20.66$ Therefore, η_{ind} =32.1 %

6. Conclusions

In this work, our interest focuses on the photovoltaic characteristics of the three modes of multi-junction solar cells made of CGS / CIGS.

The multi-junction cell systems allow the obtaining of an efficiency higher than the one obtained with the implementation of a single cell. By associating CGS with CIGS, about10% of efficiency is gained compared to using a single CIGS cell only. The maximum efficiency of 32.1% is obtained due to the strong contribution of dichroic mode independent system.

Tandem solar cells have a big defect. The contact between the cells forms a PN junction called parasite junction. The tunnel junction offers a solution because it is sensibly different from the current-tension characteristics.

References

[1] S. Niki, M. Contreras, I. Repins, M. Powalla, K. Kushiya, S. Ishizuka, K. Matsubara, Prog. Photovolt. **18**, 453 (2010).
[2]K.L. Chopra, P.D. Paulson, V. Dutta, Res. Appl. **12**, 69 (2004).
[3] J. Raman, U. P. Singh, Energy Environ. Sci. **10**, 1306 (2017).
[4] Dennai Benmoussa, H. Benslimane, H. Khachab, Energy Procedia**139**, 731 (2017).
[5] P. Jackson, D. Hariskos, E. Lotter, S. Paetel, R. Wuerz, R. Menner, W. Wischmann, M. Powalla, Res. Appl. **19**, 894 (2011).
[6] Appl. Phys. Lett, Vol. **43**, p. 468 (1983).
[7] Hongxia Wang, International Journal of Photoenergy, 2011.
[8] M.Fillali,B.Dennai, Journal of Ovonic Research ,Vol. 15, No. 5, 2019, p. 279 - 285